JRAI Journal of the Royal Anthropological Institute

The morphological affinities of the fossil cranium from Kabua, Kenya

Abel Marinus Bosman *Eberhard Karls Universität Tübingen*

Laura Tabitha Buck *Liverpool John Moores University/Eberhard Karls Universität Tübingen*

Hugo Reyes-Centeno *University of Kentucky/Uppsala University*

Marta Mirazón Lahr *University of Cambridge*

Chris Stringer *Natural History Museum*

Rainer Grün *The Australian National University/Nanjing Normal University*

Qingfeng Shao *Nanjing Normal University*

Katerina Harvati *Eberhard Karls Universität Tübingen*

Our current understanding of the origins of *Homo sapiens* is limited, in part, by the fragmented fossil record from Late Pleistocene and early Holocene Africa. Here, we re-examine the Kabua 1 cranium, an enigmatic and little-studied Kenyan fossil discovered in the 1950s. We compare virtual reconstructions created previously by our team with a wide range of Middle Pleistocene to Early Holocene fossils and recent African *H. sapiens* crania to assess Kabua 1's morphological affinities. We also provide a conservative new Uranium-series minimum date of 64.4 ± 5.4 ka. Our results highlight Kabua 1's broad similarity to derived *H. sapiens*, both recent and fossil. Its morphology nevertheless demonstrates some more basal affinities and thus contributes to our understanding of the depth of phenotypic diversity in Late Pleistocene African *H. sapiens*.

Introduction

African fossils thought to lie on the *Homo sapiens*[1] lineage are known from the Middle Pleistocene onwards, but the relationships between them remain uncertain. Several

Journal of the Royal Anthropological Institute (N.S.) **00**, *1-25*

factors contribute to this, from sample size to multiple cases of unclear stratigraphic context, unknown chronology, and taphonomic distortion. Advances in clarifying these issues and new fossil discoveries in recent years have contributed to understanding the origins and evolution of our species; yet morphologically derived models are sometimes at odds with hypotheses drawn from genetic studies of recent people (Henn, Steele & Weaver 2018). Here we expand on our previous work reconstructing and describing the Kabua 1 cranium, a fragmentary fossil from Turkana, Kenya. We quantitatively assess its morphological affinities within the context of a newly obtained chronological age to augment our understanding of anatomical diversity in *H. sapiens*.

Models of *Homo sapiens* origins

The origin of *H. sapiens* is among the most long-standing questions in evolutionary anthropology. Although today there is a general acceptance of a recent African origin (RAO), incorporating limited interbreeding with extinct taxa (Stringer 2022), debate remains over which region(s) within Africa were involved, and what evolutionary mechanisms were most influential (Harvati & Reyes-Centeno 2022; Henn *et al.* 2018; Meneganzin, Pievani & Manzi 2022; Scerri *et al.* 2018; Scerri, Chikhi & Thomas 2019). The possibility of multiple regional African contributions to *H. sapiens* origins dates back to the genesis of the RAO model (Stringer 2002; 2012*a*; 2016; 2022; Stringer & Buck 2014), and some genetic studies had also pointed to this possibility (e.g., Harding & McVean 2004), but it was formalized as the pan-African origin model by a multidisciplinary group in 2018 (Scerri *et al.* 2018). This model proposes that the origin of *H. sapiens* was a process playing out across the African continent, rather than an event occurring in a single area or population. It underlines the roles of climate and ecology, emphasizing the effects of population fragmentation and coalescence (Scerri *et al.* 2018). By a process comparable to the suggested accretion of Neanderthal characteristics in Europe (Hublin 2007), it is hypothesized that derived *H. sapiens* traits such as neurocranial globularity, a mental eminence on the mandible, and a retrognathic face arose in different regions and were transmitted and assimilated via gene flow between populations (Scerri *et al.* 2018; 2019).

The mosaic appearance of derived *H. sapiens* traits across Africa, without clear chronological progression from more-basal to more-derived in any region, is argued to demonstrate a pan-African origin (Scerri *et al.* 2018; 2019). For example, fossils often placed early in the *H. sapiens* lineage, such as those from Jebel Irhoud (Morocco, ~300 ka), Florisbad (South Africa, ~260 ka), and Omo 1 (Ethiopia, ~230 ka) are of a broadly similar geological age but display diverse morphology (Grün *et al.* 1996; Hublin *et al.* 2017; Richter *et al.* 2017; Stringer 2016; Vidal *et al.* 2022). Similarly, Late Pleistocene fossils such as Iwo Eleru (Nigeria, ~14 ka), Ishango (Democratic Republic of Congo, ~20-25 ka), and Lukenya Hill (Kenya, ~22 ka), which show some basal traits (Crevecoeur, Brooks, Ribot, Cornelissen & Semal 2016; Harvati *et al.* 2011; Harvati, Stringer & Folorunso 2024; Stringer 2016; Tryon *et al.* 2015), have been posited as evidence for the persistence of deep population structure relating to a pan-African origin (Scerri *et al.* 2018). It remains unclear, however, whether the degree of gene flow necessary for a pan-African origin is feasible given estimated population densities and why genetic data from living people seem to suggest a more recent coalescence than would be predicted if key fossils dated ~300-200 ka contribute to derived *H. sapiens* (Henn *et al.* 2018).

Competing models suggest that derived morphology, or genetic variants, originated in a single region of Africa (usually eastern/southern Africa), spreading throughout the continent with varying degrees of replacement or gene flow with incumbent populations (Bergström, Stringer, Hajdinjak, Scerri & Skoglund 2021; Chan *et al.* 2019; Henn *et al.* 2018; Meneganzin *et al.* 2022; Ragsdale *et al.* 2023; Schlebusch *et al.* 2021). In these models, individuals with derived characteristics outside of the key region and Late Pleistocene individuals with more basal features are often viewed as branches that ultimately did not contribute to our lineage. Genetic analyses provide some support for such models, such as the low effective population size estimated for the ancestral population, relatively recent (<300 ka) estimates of the earliest population divergence based on recent humans, and the great diversity found in the KhoeSan people of South Africa (Henn *et al.* 2018). Opponents of replacement models have argued that the lack of a discernible pattern of increasingly derived morphology in the fossil record of any one region is evidence against them, but it is far from clear that there is currently a sufficient sample to make such a determination.

While such competing models of *H. sapiens* origins have recently begun to be tested using genetic, archaeological, and fossil data (e.g., Cousins, Scally & Durbin 2025; Henn *et al.* 2018; Ragsdale *et al.* 2023), we currently lack the power to distinguish them due, at least in part, to the limited palaeoanthropological record (Harvati & Reyes-Centeno 2022). The paucity of the fossil evidence can be ameliorated by applying newly developed digital techniques to reconstructing and reanalysing previously discovered fragmented or distorted fossils and identifying their geochronological context. One such potentially valuable and understudied fossil is Kabua 1.

The morphology of Kabua 1

For a complete description of Kabua 1, see Bosman *et al.* (2019). The fossil is represented by frontal, parietal, occipital, temporal, maxillary, and mandibular fragments, and several teeth (Figure 1). The fossil's morphology is enigmatic: Whitworth, who discovered the fossil (Whitworth 1960; 1966), described it as possessing basal characteristics including a long, narrow neurocranium with very thick vault walls, a sloping frontal, and a very robust mandible. He also noted, however, the presence of a chin, a derived *H. sapiens* trait, and queried the effects of post-mortem distortion on the vault shape (Whitworth 1960; 1966). Later authors have tended to attribute the morphology of Kabua 1 to the wide range of derived *H. sapiens* variation seen in eastern Africa during the early Holocene (Rightmire 1975; Schepartz 1987), whilst investigation of the bony labyrinth reveals both basal and derived traits (Reyes-Centeno, Buck, Stringer & Harvati 2014).

Working with new microCT data, we recently published virtual reconstructions of Kabua 1 using reference crania from a range of Pleistocene and recent African individuals (Bosman *et al.* 2019). This qualitative assessment of our reconstructions suggested that Kabua 1 has a relatively globular neurocranium and that reconstructions based on recent Holocene *H. sapiens* references (two Maasai individuals) had the greatest anatomical congruence, whereas more basal *H. sapiens* (Ngaloba) and the Middle Pleistocene fossil Kabwe (Broken Hill) 1 produced less plausible reconstructions (Bosman *et al.* 2019). Here, we build on this description and use geometric morphometric techniques to thoroughly and quantitatively evaluate the position of the Kabua 1 reconstructions relative to other African hominin fossils from the Mid-Late Pleistocene and to a wide sample of recent African *H. sapiens*. We focus on

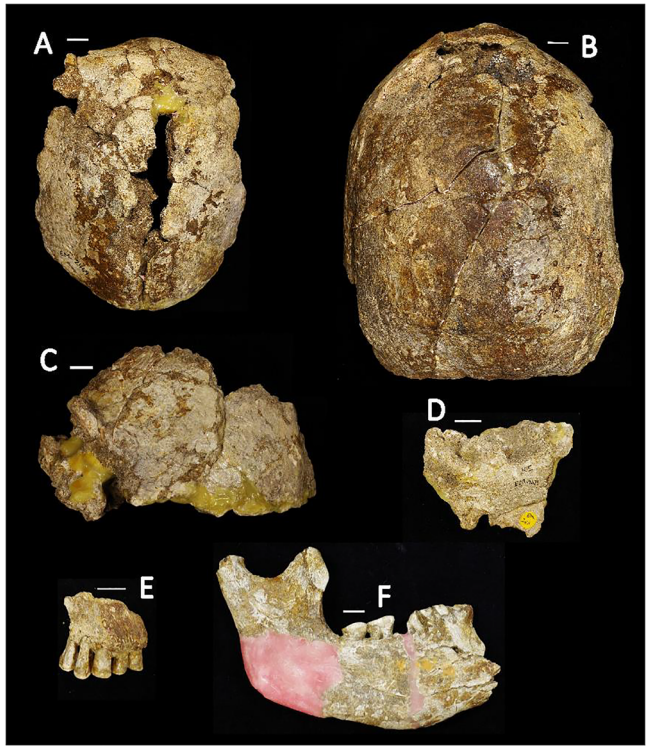

Figure 1. Photographs of cranial fragments used in virtual reconstructions of Kabua 1. A: EM.2469: frontal in *norma verticalis*; B: EM.2468, occipitals and parietals in *norma occipitalis*; C: EM.2470, left temporal including parietal fragment in *norma lateralis*; D: EM.2471, right temporal in inferolateral view with anterior facing left; E: EM.2481 maxillary fragment, buccal view with anterior facing right; F: EM.2480, right hemimandible. Scale bars = 1cm. Photos courtesy of the Natural History Museum, London.

the neurocranium as it has been shown to capture the signature of neutral evolution (Athreya 2009; Harvati & Weaver 2006; Hubbe, Hanihara & Harvati 2009), its globularity is one of the most taxonomically diagnostic characteristics of *H. sapiens* (Meneganzin *et al.* 2022; Mirazón Lahr 1996; Stringer & Buck 2014; Stringer, Hublin & Vandermeersch 1984), and since it is the most complete region of Kabua 1 (Bosman *et al.* 2019; Phenice & Sauer 1977; Rightmire 1975; Schepartz 1987).

Materials

Kabua 1 reconstructions

The virtual reconstruction of Kabua 1 is described in detail in Bosman *et al.* (2019). In short, following microCT scanning and mirroring missing material, the fragments of Kabua 1 were virtually reassembled based on their anatomy and the geometry of the fractures between them. Six reference crania (Table 1) were used to aid the reconstruction, resulting in six reconstructions (Weber & Bookstein 2011). These reference crania encompassed a range of taxa, morphology, and a wide chronological spread, reflecting the uncertainty surrounding Kabua 1's place in the fossil record. This enables us to discuss Kabua 1's likely affinities as a distribution of possible morphology, which is more plausible than relying on a single model and its inherent assumptions.

Table 1. Summary of crania used as references for the virtual reconstructions of Kabua 1 (Bosman *et al*. 2019).

	Kabwe 1	LH18 / Ngaloba	Skhūl 5	Mumba X	Maasai 3	Maasai 10
Locality	Kabwe, Zambia	Laetoli, Tanzania	Mount Carmel, Israel	Mumba-Höhle, Tanzania	Northeast Lake Eyasi	Northeast Lake Eyasi
Taxon	*H. rhodesiensis / H. heidelbergensis* sensu lato[a]	*H. sapiens*	*H. sapiens*	*H. sapiens*	Recent *H. sapiens*	Recent *H. sapiens*
Estimated age (years)[b]	~300,000	~120,000	130,000-100,000	>5,000	<500	<500
Basis for dating estimate	U-series dating	Amino-acid racemization, association with artifacts/faunal remains, Ar/Ar dating	U-series, ESR	Associated C_{14} dating of Mumba IX in the same layer (Mumba X lies lower in the sequence and is more mineralized)	Associated C_{14} date of charcoal found with Maasai 1[c]	Associated C_{14} date of charcoal found with Maasai 1[c]

[a] It should be noted that the taxonomic position of Kabwe 1 is much disputed, as is the validity and hypodigm of the taxon of which it is the holotype: *H. rhodesiensis*, and which it is often attributed to, *H. heidelbergensis* (Athreya & Hopkins 2021; Buck & Stringer 2014; Delson & Stringer 2022; Harvati 2007; Harvati & Reyes-Centeno 2022; Hautavoine, Arnaud, Balzeau & Mounier 2024; Roksandic, Radović, Wu & Bae 2022; Stringer 2012*b*). Here, Kabwe 1 is used as a representative of a non-*H. sapiens*, Middle Pleistocene taxon as a contrast to the recent *H. sapiens* individuals, to provide a wide range of morphological comparisons for Kabua 1.

[b] Estimated or determined dates: Kabwe: Grün *et al*. (2020); Ngaloba: Day, Leakey and Magori (1980); Skhūl 5: Grün *et al*. (2005); Mumba and Maasai: Bräuer (1976) and Mehlman (1979).

[c] Maasai 1 is another individual from the same burial site as Maasai 3 and 10, which is not included in this study.

Comparative data

For the new quantitative analyses presented here, our comparative sample (Table 2) comprises several Pleistocene hominin fossils from Africa and Eurasia and a large sample of recent African *H. sapiens* individuals. The specimens are housed at the institutions listed in the Acknowledgements. The fossil landmark dataset was primarily collected using a MicroScribe G2X portable digitizer (Immersion Corporation 1998) by Harvati and is a subsample from Harvati *et al.* (2011; see also Harvati, Gunz & Grigorescu 2007; Harvati 2009). Additional Pleistocene fossils were digitized in Avizo Lite 9.0 (Thermo Fisher Scientific 2019) by Buck for this study. The remainder of the comparative dataset consists of 109 recent *H. sapiens* crania from eastern and southern Africa, collected using a MicroScribe by Harvati and Reyes-Centeno. All the crania were adult, and, for the recent *H. sapiens* sample, no pathological specimens were included. Due to the limited potential fossil sample, Singa (Spoor, Stringer & Zonneveld 1998) was included despite showing evidence of neurocranial pathology, and the influence of this pathology on Singa's morphology was considered.

When conducting classificatory analyses of morphological affinity, the choice and definition of taxa unavoidably influence the results. Since the taxonomy of Mid-Late Pleistocene hominins is very far from settled, here we used only very broad, demic groups (Howell 1999) to ascertain whether geometric morphometric analysis supports early assertions that Kabua 1 shows basal characteristics (Whitworth 1966), or if it is indistinguishable from derived *H. sapiens* (Rightmire 1975; Schepartz 1987).

Landmark data

We used Avizo Lite version 9.0 (Thermo Fisher Scientific 2019) to digitize six fixed landmarks and two curves of semi-landmarks (Table 3) on each Kabua 1 reconstruction and on the comparative sample (Table 2). The landmarks and semi-landmarks were chosen to characterize neurocranial morphology as completely as possible given the preservation of our sample. For the comparative sample, where necessary, the dorsal-ventral-left-right fitting program (DLVR; http://pages.nycep.org/nmg/programs.html) was used to process MicroScribe-derived data. Subsequently, Resample software (http://pages.nycep.org/nmg/programs.html) was used to create semi-landmark curves of equal numbers of equidistant semi-landmarks using weighted linear interpolation. Missing landmarks and semi-landmarks (SI Table 2 in the Supporting Information) were reconstructed by reflected relabelling of their bilateral homologue (Mardia & Jupp 2000) in Morpheus (https://morphlab.sc.fsu.edu/software/morpheus/index.html), or by applying a function based on the publication by Claude (2008) in R, version 3.5.0 (R Core Team, 2019). All subsequent data preparation steps and analyses were also performed in R.

Methods

Dating the Kabua 1 fossil

Because a radiometric date for the Kabua fossils has previously been elusive (for a summary, see Bosman *et al.* 2019), here we undertook new Uranium (U)-series dating. Three samples were retrieved directly from Kabua 1 (Table 4): Australian National University lab number 2931 (Natural History Museum (London) catalogue number EM2468) – biparietal portion-occipital; 3528 (EM2480) – a partial molar from the mandible; and 3534 (EM2471) – a larger, dense sample from the temporal bone fragment. In addition, comparative samples 3527 (EM2472) and 3535 (EM2474)

Table 2. Complete sample for the geometric morphometric analyses.

Group	n	Specimens[a]
Middle Pleistocene Eurasians (MPE)	3	Dali (Dali)[b], Sima de los Huesos 5 (SH05), Petralona (Petr)
Middle Pleistocene Africans (MPA)	4	Kabwe/Broken Hill 1 (BrH)[c], Saldanha (Sald), Jebel Irhoud 1 (Iro1), Jebel Irhoud 2 (Iro2)
H. neanderthalensis (NEA)	8	Amud 1 (Amo1), Feldhofer 1 (Fel1)[b], Guattari 1 (Gua1)[c], La Chapelle-aux-Saints 1 (LaC1), La Ferrassie 1 (LaF1), La Quina 5 (LQn 5), Spy I (Spo1), Spy II (Spo2)
H. sapiens (HSA)	130	
Late Pleistocene	21	Afalou 12 (AF12)[c], Brno 2 (BRN2), Cro-Magnon 1 (CRM1), Cro-Magnon 2 (CRM2), Cro-Magnon 3 (CRM3), Dolní Věstonice 3 (DV03), Dolní Věstonice 13 (DV13), Dolní Věstonice 15 (DV15), Dolní Věstonice 16 (DV16), Mumba 10 (Mumb)[c], Nazlet Khater 2 (NZKH), Ngaloba / LH18[c], Pavlov 1 (PAV1), Predmosti 3 (PRD3)[b], Predmosti 4 (PRD4)[b], Qafzeh 9 (Qa09), Skhūl 5 (Skl5), Taforalt 11 C1U (IT11)[c], Taforalt 15 C4U (IT54)[c], Taforalt 15 C5U (IT55)[†], Taforalt 18 C1U (IT18)[c]
Holocene	109	Amhara ($n = 2$; AM), Danakil ($n = 2$; DA), Ethiopian ($n = 10$; ET), Igai ($n = 1$; IGAI), Kenya ($n = 3$; Ke), Kokoro ($n = 1$; Koko), Maasai ($n = 2$; MA)[c], Pouma ($n = 1$; Poum), San from Museum of Cape Town ($n = 54$; SA), San from University of Cape Town ($n = 7$; UC), Somalia ($n = 1$; Soma), Turkana ($n = 2$; TU), Zulu ($n = 23$; ZU)
Kabua reconstructions	6	Kabua-Broken Hill (K-BrH), Kabua-Ngaloba (K-LH18), Kabua- Skhūl V (K-Skl5), Kabua-Mumba X (K-Mumb), Kabua-Maasai 3 (K-Mao3), Kabua-Maasai 10 (K-Ma10)

[a] Abbreviated names used in figures follow specimen names in parentheses. The reconstructions of Kabua 1 are labelled by their relevant reference specimen (Table 1) following the prefix "K-".
[b] Specimens for which high-quality casts or stereolithographs were measured.
[c] Specimens for which we had access to CT-data.

Table 3. Landmarks used in this study and their description.

Landmark	Description
Inion	Point at which the superior nuchal lines merge at the midline
Asterion (B[a])	Meeting point of the temporal, parietal, and occipital bones
Parietal notch (B)	Point on the posterosuperior border of the temporal where the squamosal and parietomastoid sutures meet
Glabella	Most anterior midline point on the frontal bone
Semi-landmark curves	
Midsagittal profile	26 semi-landmarks, from glabella to inion
Lambdoid suture (B)	14 semi-landmarks from asterion (right) to lambda to asterion (left), along lambdoid suture

[a] B: bilateral landmarks.

Table 4. Samples analysed for U-series dating, see Figures 1 and 2.

ANU lab sample number	NHM catalogue number	Description
2931	EM 2468	Kabua 1 biparietal-occipital portion (analysed in 2011)
3528	EM 2480	Partial M2 in situ in Kabua 1 mandible
3534	EM 2471	Kabua 1 temporal fragment
3527	EM 4272	Kabua 2
3535	EM 2474	Kabua 2
3529DE		Hippo tooth
3530DE		Hippo tooth

ANU: Australian National University; NHM: Natural History Museum, London.

originating from Kabua 2 (a separate, much more fragmentary individual [Whitworth 1960; 1966]) and two hippo tooth fragments (3529DE and 3530DE) found in the vicinity of the human skeletal remains were also sampled. Sample 2931 (EM2468), the large fragment of Kabua 1 cranium, was analysed in 2011, while the remainder were studied in 2014.

Laser ablation analyses were carried out at the Australian National University's Environmental Geochemistry laboratory. The analyses followed the procedures described in detail by Grün, Eggins, Kinsley, Moseley & Sambridge (2014). U-series results on bones are generally regarded as minimum age results, and thus all individual age estimates reported here are apparent closed system ages. All isotope ratios are activity ratios with 2-σ errors; elemental ratios are concentration ratios.

Geometric morphometric methods

To compare the reconstructions of Kabua 1 to each other and to the comparative sample, we first used the *geomorph* R package (Adams & Otárola-Castillo 2013) to superimpose the landmark set using generalized Procrustes analysis and to slide the semi-landmarks by minimizing bending energy (Gunz, Mitteroecker, Neubauer, Weber & Bookstein 2009; Perez, Bernal & Gonzalez 2006). We analysed the coordinates of the Procrustes aligned landmarks using principal component analysis (PCA) and classification procedures comprising linear discriminant analysis (LDA), and two machine learning algorithms: *k*-nearest neighbour (*k*-NN; Ripley 1996) and random forest (RF; Breiman 2001) modelling (details in section 2 of the Supporting Information).

The PCA was performed in *geomorph* on the comparative sample and the reconstructions projected into the PC shape space. The PCA figures were created using *ggplot2* (Wickham 2016). Shape differences illustrating the maximum and minimum range of each PC were visualized using thin plate spline relative warps (Bookstein 1989). The Auer-Gervini method (Auer & Gervini 2008; Wang, Kornblau & Coombes 2018) was used to retrieve the number of significant principal components. We also computed a neurocranial shape index (Gunz *et al.* 2009; Harvati *et al.* 2019) using the mean PC scores of the Neanderthal and *H. sapiens* groups and projecting all other specimens onto this axis. LDA was performed on significant PCs, with equal prior probabilities for all groups and jackknife cross-validation. All classification analyses were run with the *caret* package (Kuhn 2007; 2008), with dependencies in the *ranger* (Wright & Ziegler 2017) and *MASS* (Venables & Ripley 2002) packages in R.

Results

Radiometric chronology

The dating results indicate a complex sequence of uranium migration processes and will be published in detail elsewhere. Here we discuss only the Kabua 1 samples (Table 4), while the results from other samples are used to infer U-migration processes. The analytical results of the Kabua 1 tooth, sample (ANU lab number) 3528, are shown in an isotope evolution diagram in Figure 2A, while those of the other samples are shown in Figure 2B along with a plot of U-concentration against their $^{230}Th/^{234}U$ ratios. Because of the relatively low U-concentrations, the analytical errors are large, and one can only observe general trends. The $^{234}U/^{238}U$ ratios give an indication for the isotopic composition of the U-source, whereas the $^{230}Th/^{234}U$ ratios are a measure of time. The diagrams also contain the equilibrium line. If the sample is a closed system and the isotopes in the sample change their composition purely by decay, the measured $^{230}Th/^{234}U$ ratio cannot cross the equilibrium line to the right (within error). Results to the right can only occur through U-leaching. More recent U-overprints shift the isotope ratios to the left. While leaching affects the $^{234}U/^{238}U$ little (i.e., the shift to the right follows a more or less horizontal line), secondary overprints shift the $^{234}U/^{238}U$ ratios towards the composition of the younger U-source (if it is different from the original composition). Leaching is associated with U-loss, secondary overprints with increased U-concentrations.

In the simplest terms, the sequence of the uranium mobilization events in the Kabua 1 dental sample (3528) can be postulated as follows: there was an initial U-accumulation event from a uranium source with a $^{234}U/^{238}U_0$ composition somewhat higher than 1.65. At some time afterwards, a leaching event took place affecting the whole tooth. After leaching ceased, a secondary overprint took place from a U-source with a $^{234}U/^{238}U_0$ composition of around 1.34, which is very much in the range of the other bone samples from Kabua, as well as of the dentine of the two hippos (Figure 2B). This means that all finite ages in sample 3528 are the result of at least three different U-mobilization events. More complex scenarios are possible (and probable), particularly in view of the fact that these mobilization processes take place over varied time spans (which can be more or less instantaneous on a geological scale – perhaps within a couple of thousand years – or proceed over tens of thousands of years). As such, it is not possible to derive a reasonable minimum age for the sample 3528 tooth from the Kabua 1 mandible.

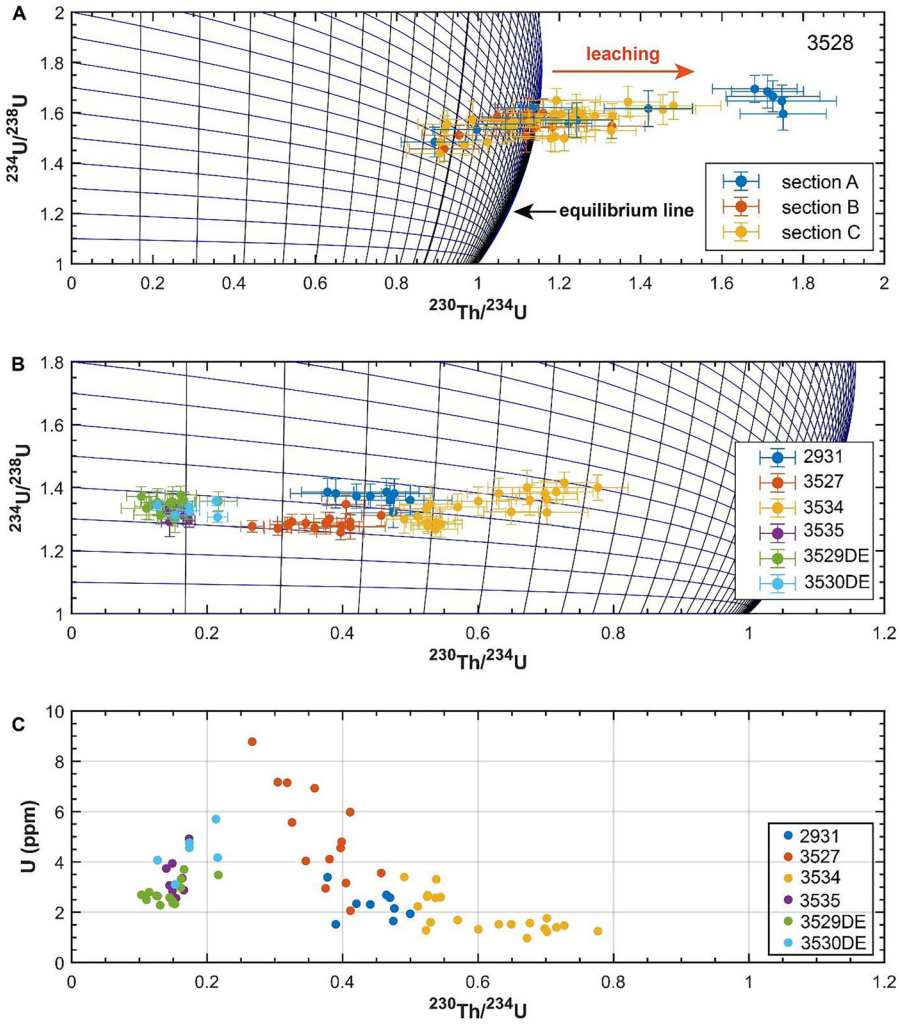

Figure 2. Graphs showing Uranium-series dating results. For key to sample numbers, see Table 4, for explanation of results, see text. Figure by the authors.

The analytical results of the Kabua 1 bone samples (ANU lab numbers 2931 and 3534), along with those of the dentine of the two hippos, are shown in an isotope evolution diagram in Figure 2B and their U-concentrations are plotted against the $^{230}Th/^{234}U$ ratio in Figure 2C. There is no overlap with the results from the Kabua 1 tooth (sample 3528; cf. Figures 2A and 2B). Considering all the samples from Kabua, there are clear trends of increasing U-concentrations with decreasing $^{230}Th/^{234}U$ ratios in samples 3527 and 3534. Samples 2931, 3535, 3529DE, and 3530DE do not show obvious trends and the scatter is most probably due to the low precision of the measurements indicating single stage U-accumulation events. The composition seems to have changed over time with a $^{234}U/^{238}U_0$ of around 1.5 for the sample of Kabua 1 temporal fragment (3534) (~114 ka), 1.45 for the biparietal-occipital sample of Kabua 1 (2931)

(∼ 65 ka), reaching around 1.35 after 50 ka (non-Kabua 1 samples: 3527, 3535, 3529DE and 3530DE). This U-source seems responsible for the more recent observed overprints in samples 3527, 3534 and 3538.

One of the bone samples from Kabua 1, from the biparietal-occipital fragment (2931) indicates a minimum age of ∼65 ka, while the second one, from the temporal (3534) reaches 114 ka. As can be seen from the detailed analysis, the U-migration processes are complex, with both U-overprinting and leaching documented. It is therefore not surprising that different fragments of one individual would yield different U-series age estimates; this age is related to the U-uptake process, which may happen a long time after the individual joins the fossil record. Assuming the Kabua 1 samples come from the same individual, the best minimum date is provided by sample 3534 with 114 ka. This sample is relatively large and dense, and thus macroscopically by far best suited for the analysis. Without having measured sample 3528 (the Kabua 1 dental sample), this would be the most straightforward interpretation of the data obtained from the bone samples from Kabua 1. We have seen, however, that in the past a massive leaching event has taken place. It is in principle possible that the pattern in sample 3534 (from Kabua 1 temporal fragment) was also partly the result of leaching, that the sample had initially acquired an isotopic composition similar to sample 2931 (from the Kabua 1 biparietal-occipital fragment), and the reduced U-concentrations were caused by leaching. As we have seen in the dentine of sample 3528, the mobilization processes affected the whole volume of the specimen. Sample 2931 was most likely not affected by leaching, as all younger samples have lower $^{234}U/^{238}U$ ratios. Conservatively, therefore, the minimum age for Kabua 1 would be derived from the large biparietal-occipital fragment, sample 2931, giving 64.4 ± 5.4 ka.

Ordination of the affinities of the Kabua 1 reconstructions

The PCA shows that the greatest variation within our sample (PC1; 26.9% variance) reflects differences in neurocranial shape from low and elongated at the minimum extent, to rounded and anteroposteriorly short (i.e., globular) at the maximum extent, in agreement with previous analyses of neurocranial shape (e.g., Harvati 2009; Harvati *et al.* 2007, 2011, 2019; Harvati & Ackermann 2022; Figure 4). Crania with negative scores on PC1 also have mediolaterally wide lambdoid sutures, resulting in a more circular occipital outline in posterior view, whereas at positive scores on PC1 the lambdoid suture is more acutely angled, resulting in a more ovoid occipital. Neanderthals and Middle Pleistocene hominins have relatively low scores on PC1, reflecting their generally elongated neurocrania and, in the case of the Neanderthals, their 'en bombe' occipital morphology. *H. sapiens* are situated predominantly on the positive side of PC1, demonstrating more globular neurocrania. The Kabua 1 reconstructions all score relatively highly on PC1, falling within the range of *H. sapiens* variation and reflecting relatively globular neurocrania.

The second principal component (16.5% total variance) does not clearly differentiate between taxa but represents intragroup variation. Crania with negative scores display a less vertical frontal and a relatively straight curve between lambda and inion. Mediolaterally, these crania have wide shapes, with the lambdoid suture located relatively inferiorly, resulting in a square-shaped occipital in posterior view. Crania with positive scores on PC2 show more vertically oriented frontals and mediolaterally narrower vaults (Figure 3). Variation within Neanderthals and *H. sapiens* encompasses nearly the whole of PC2, with the Middle Pleistocene hominins more localized on the

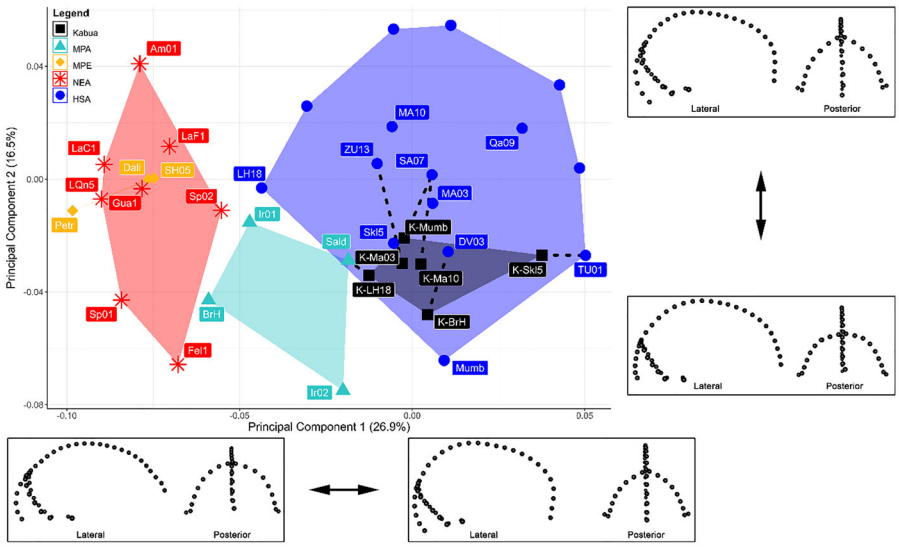

Figure 3. PCA of comparative sample with Kabua 1 reconstructions projected. In the *H. sapiens* (HSA) group, only nearest neighbours to reconstructions and reference crania are depicted and labelled, joined by dashed line. Abbreviations as in Table 2. For more information on nearest neighbours, see main text and Table 5. Figure by the authors.

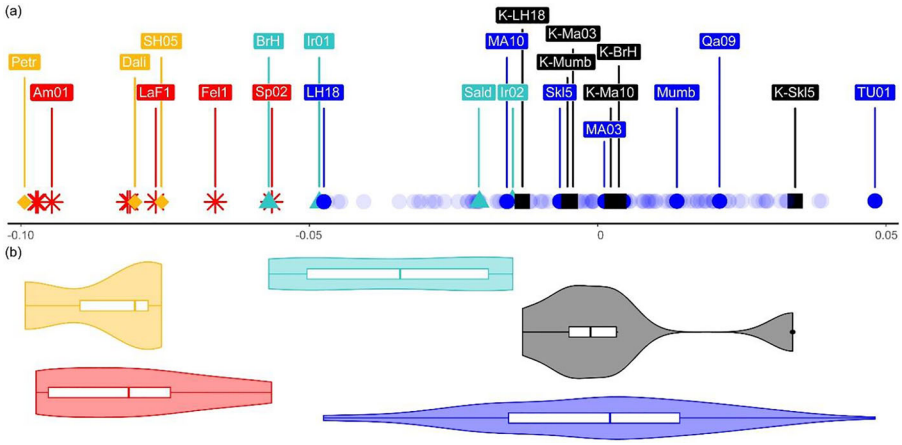

Figure 4. (a) Neurocranial shape index (Gunz *et al.*, 2019; Harvati *et al.* 2019). Symbols and colours as in Figure 3, abbreviations as in Table 2. *H. sapiens* have their opacity reduced in order to increase readability. (b) Violin plots reflecting the variation in (a). Whiskers of boxplots show minimum and maximum values of the calculated shape indices per group, internal boxes show 25-75% quartiles, and lines in boxes show median values. In this visualization, the Kabua 1 reconstructions are treated as a group, in which the Kabua reconstruction based on Skhūl 5 can be considered an outlier (filled circle on far right of black violin). Figure by the authors.

negative side due to their low lambdoid sutures and short nuchal planes. The Kabua 1 reconstructions also score low on PC2, overlapping with Middle Pleistocene hominins and Neanderthals as well as some *H. sapiens*. This reflects a short nuchal plane, less vertical frontal, and mediolaterally narrow neurocranium.

Table 5. Procrustes distances between reconstructions of Kabua 1 and their respective reference crania.

Reconstruction[a]	Distance to reference[b]	Count of reference[c]	Closest neighbour[d] (specimen; group)
K-BrH	0.086	52nd	DV03; HSA
K-Ma03	0.070	11th	ZU13; HSA
K-Ma10	0.083	39th	MA03; HSA
K-Mumb	0.096	69th	SA07; HSA
K-LH18	0.088	46th	Sal1; MPA
K-Skl5	0.082	35th	Tur1; HSA

DV: Late Pleistocene site of Dolní Věstonice; ZU: Holocene Zulu; MA: Holocene Maasai; SA: Holocene South African; Tur: Holocene Turkana.
[a] Abbreviations as in Table 2.
[b] Procrustes distance value from Kabua 1 (K) to reference specimen.
[c] Count of reference indicates the position of the reference crania Procrustes distances to that of the reconstruction in the context of the distances to all individuals, these are ordered from lowest to highest.
[d] Closest neighbours indicated in this table exclude other reconstructions. See also dashed lines in Figure 3.

When considering the combined variation of PC1 and PC2 (~43% variation), all the reconstructions of Kabua 1 are within the *H. sapiens* range, as delimited by a convex hull (Mitteroecker & Bookstein 2011). The Ngaloba-based reconstruction is closest to the Middle Pleistocene African group, close to where Middle Pleistocene African fossil Saldanha overlaps with the *H. sapiens* group, but still within the *H. sapiens* convex hull. The Skhūl 5-based reconstruction is distinct from the other Kabua 1 reconstructions, being near the maximum value of PC1, corresponding to the markedly globular shape of its neurocranium. The other four reconstructions all plot relatively close to one another between these two extremes.

All the reconstructions of Kabua 1 have another reconstruction as their closest neighbour, and the reconstruction based on Maasai 03 is a basal node of all reconstructions (Table 5, Figure 3). The majority of other (non-Kabua reconstruction) closest neighbours for the Kabua 1 reconstructions are *H. sapiens* (Table 5). The exception is the reconstruction based on Ngaloba (LH18), which, similarly to what is observed in the PCA (Figure 3), is closest to the African Middle Pleistocene fossil Saldanha. None of the reconstructions is particularly close to their respective reference crania in either PCA morphospace or shape space (i.e., Procrustes distance), showing that the reconstructions each reflect interpretations of the Kabua 1 morphology, rather than only that of their reference (Table 5).

The neurocranial shape index (Figure 4) separates *H. sapiens* and older Eurasian specimens. The Neanderthal and Middle Pleistocene Eurasian groups are located low on this axis, whilst *H. sapiens* is more positively positioned. The Middle Pleistocene African group is intermediate, with substantial overlap with *H. sapiens*. All the Kabua 1 reconstructions are within the range of *H. sapiens*. The reconstruction based on Ngaloba is closest to the Middle Pleistocene African group, while the reconstruction based on Skhūl 5 is towards the maximum of the axis, reflecting the variation in neurocranial shape between Kabua 1 reconstructions shown in the PCA (Figure 3).

Classification of the Kabua 1 reconstructions

The linear discriminant analysis (jackknife classification of comparative sample = 93.8%, Cohen's kappa = 0.687) classifies all the Kabua 1 reconstructions

Table 6. Posterior probabilities for the linear discriminant analysis. The posterior probabilities for Middle Pleistocene Eurasian and Neanderthal groups were close to 0 and were therefore excluded.

	Group	K-BrH	K-Ma03	K-Ma10	K-Mumb	K-LH18	K-Skl5
	MPA	0.958	0.694	0.910	0.997	0.994	0.004
	HSA	0.031	0.443	0.127	0.077	0.004	0.998
Result		MPA	MPA	MPA	MPA	MPA	HSA

Abbreviations as in Table 2.

as Middle Pleistocene Africans with the exception of that based on Skhūl 5, which is classified as *H. sapiens* (Table 6). The Procrustes superimposed coordinates of the comparative sample show high measures of skewness (−9081.82) and kurtosis (692.83), as tested using Mardia's test of multivariate normality. This is due to the non-normal distribution of this high-dimensional dataset (section 5 in the Supporting Information). We therefore used a systematic stopping rule (Auer-Gervini) to estimate the statistical significance of the PCs extracted, resulting in the first 12 PCs (explaining 85.2% of variance) being significant. Tests for univariate normality (SI Table S3 in the Supporting Information) and multivariate normality (Mardia skewness = 668.53, $p < 0.01$; Mardia kurtosis 5.57, $p < 0.01$) on the significant PCs show that these scores also deviate from a normal distribution (Figure S3 in the Supporting Information) and the sample contains several outliers, notably: Feldhofer 1, Amud 1, Spy 1, Jebel Irhoud 1, Jebel Irhoud 2, and Petralona (Figure S4 in the Supporting Information). The Kaiser-Meyer-Olkin test returns a mediocre overall measure of sampling adequacy of 0.68, while the Fligner-Killeen test (1976) shows overall homogeneity of variance among groups ($Chi^2 = 15.557$, df = 9, p-value = 0.077).

Results from the *k*-nearest neighbour algorithms with different sample sizes of *H. sapiens* vary slightly. When the *H. sapiens* sample is randomly subsampled to three or four individuals, all of the reconstructions are classified as Middle Pleistocene African, with the exception of that based on Skhūl 5, which is classified as *H. sapiens* (*H. sapiens* $n = 3$, classification of 62.4%, Cohen's kappa = 0.378; *H. sapiens* $n = 4$, classification of 62.8%, Cohen's kappa = 0.403). When the *H. sapiens* sample size is increased to eight randomly subsampled individuals, the reconstructions based on Kabwe1 and Ngaloba are classified as Middle Pleistocene African, whilst all the other reconstructions classify as *H. sapiens* (classification of 68.6%, Cohen's kappa = 0.550). Finally, when *H. sapiens* is resampled to ten individuals, all reconstructions are classified as *H. sapiens*, with the exception of that based on Ngaloba, which is classified as Middle Pleistocene African (classification of 73.1% Cohen's kappa = 0.599; Table 7).

As with the *k*-nearest neighbour analyses, the four random forest models using the Procrustes superimposed coordinates also yield somewhat diverging results. A random subsample of three *H. sapiens* results in the Kabua 1 reconstructions classifying as Middle Pleistocene African (classification of 67.8%, Cohen's kappa = 0.379). Increasing the subsample to four *H. sapiens* individuals similarly results in Middle Pleistocene African classifications for all reconstructions except that based on Skhūl 5 (classification of 69.4%, Cohen's kappa = 0.466). A further increase in the random subsampling to eight or ten *H. sapiens* individuals, however, leads to classification of all reconstructions as *H. sapiens*, with the exception of that based on Ngaloba (*H. sapiens* $n = 8$, classification of 68.5%, Cohen's kappa = 0.524; *H. sapiens* $n = 10$, classification of 72.9%, Cohen's kappa = 0.581; Table 8).

Table 7. Posterior probabilities[a] for *k*-nearest neighbour analyses.

Method[b]	Group	K-BrH	K-Mao3	K-Ma10	K-Mumb	K-LH18	K-Skl5
k-NN A	MPA	0.741 ±0.197	0.706 ±0.242	0.687 ±0.214	0.677 ±0.237	0.85 ±0.186	0.347 ±0.102
HSA = 3	HSA	0.259 ± 0.197	0.294 ±0.242	0.313 ±0.214	0.323 ±0.237	0.150 ±0.186	0.653 ±0.102
Result		MPA	MPA	MPA	MPA	MPA	RHS
k-NN B	MPA	0.689 ±0.204	0.628 ±0.253	0.621 ±0.220	0.598 ±0.241	0.811 ±0.201	0.315±0.090
HSA = 4	HSA	0.311 ±0.204	0.372 ±0.253	0.379 ±0.220	0.402 ±0.241	0.189 ±0.201	0.685 ±0.09
Result		MPA	MPA	MPA	MPA	MPA	RHS
k-NN C	MPA	0.509 ±0.221	0.410 ±0.192	0.415 ±0.184	0.400 ±0.158	0.648 ±0.220	0.186 ±0.166
HSA = 8	HSA	0.491 ±0.221	0.590 ±0.192	0.585 ±0.184	0.600 ±0.158	0.352 ±0.220	0.814 ±0.166
Result		MPA	RHS	RHS	RHS	MPA	RHS
k-NN D	MPA	0.448 ± 0.219	0.359 ± 0.168	0.363 ± 0.162	0.355 ± 0.128	0.598 ± 0.214	0.136 ± 0.164
HSA = 10	HSA	0.552 ± 0.219	0.641 ± 0.168	0.637 ± 0.162	0.645 ± 0.128	0.402 ± 0.214	0.864 ± 0.164
Result		RHS	RHS	RHS	RHS	MPA	RHS

Abbreviations as in Table 2.

[a] Posterior probabilities for the *k*-nearest neighbours (*k*-NN) here are mean probabilities and their standard deviations over 1,000 iterations. There were no posterior probabilities for Middle Pleistocene Eurasian and Neanderthal groups, and so they were excluded.

[b] In order to account for sample size bias, each analysis has a different class size of the *H. sapiens* group (see Methods section). For example, *k*-NN A has a reference class size of 3 HSA (HSA = 3) individuals selected at random.

Table 8. Posterior probabilities[a] for random forest (RF) models.

Method[b]	Group	K-BrH	K-Mao3	K-Ma10	K-Mumb	K-LH18	K-Skl5
RF A	MPA	0.546 ±0.061	0.529 ±0.061	0.502 ±0.061	0.495 ±0.058	0.544 ±0.056	0.461 ±0.074
RHS = 3	MPE	0.066 ±0.024	0.092 ±0.029	0.088 ±0.029	0.100 ±0.030	0.089 ±0.028	0.050 ±0.022
	NEA	0.129 ±0.035	0.119 ±0.035	0.123 ±0.036	0.152±0.039	0.189 ±0.042	0.081 ±0.030
	RHS	0.259 ±0.063	0.260 ±0.067	0.286 ±0.066	0.253 ±0.062	0.178 ±0.056	0.408 ±0.080
Result		MPA	MPA	MPA	MPA	MPA	MPA
RF B	MPA	0.549 ±0.070	0.528 ±0.072	0.505 ±0.071	0.497 ±0.070	0.562 ±0.064	0.436 ±0.085
RHS = 4	MPE	0.064 ±0.026	0.090 ±0.029	0.084 ±0.029	0.100 ±0.031	0.084 ±0.028	0.045 ±0.022
	NEA	0.102 ±0.036	0.079 ±0.031	0.081 ±0.032	0.108 ±0.038	0.153 ±0.042	0.05 ±0.025
	RHS	0.285 ±0.072	0.304 ±0.078	0.330 ±0.076	0.295 ±0.073	0.201 ±0.064	0.469 ±0.089
Result		MPA	MPA	MPA	MPA	MPA	RHS
RF C	MPA	0.455 ±0.070	0.403 ±0.076	0.377 ±0.073	0.386 ±0.072	0.488 ±0.064	0.229 ± 0.075
RHS = 8	MPE	0.053 ±0.023	0.067 ±0.028	0.060 ±0.026	0.070 ± 0.027	0.070 ±0.027	0.021 ± 0.016
	NEA	0.087 ±0.032	0.066 ±0.028	0.065 ±0.029	0.086 ±0.033	0.136 ±0.039	0.026 ± 0.019
	RHS	0.405 ±0.083	0.464 ±0.093	0.498 ±0.090	0.458 ± 0.091	0.306 ±0.076	0.724 ± 0.087
Result		MPA	RHS	RHS	RHS	MPA	RHS
RF D	MPA	0.430 ±0.073	0.368 ±0.080	0.344 ±0.077	0.357 ±0.074	0.464 ±0.067	0.179 ±0.070
RHS = 10	MPE	0.051 ±0.023	0.062 ±0.027	0.057 ±0.026	0.065 ±0.027	0.067 ±0.027	0.017 ±0.015
	NEA	0.087 ±0.033	0.062 ±0.027	0.061 ±0.026	0.081 ±0.031	0.131 ±0.036	0.022 ±0.017
	RHS	0.433 ±0.091	0.508 ±0.100	0.538 ±0.094	0.497 ±0.095	0.338 ±0.084	0.781 ±0.083
Result		RHS	RHS	RHS	RHS	MPA	RHS

Abbreviations as in Table 2.

[a] Posterior probabilities for the random forest models given here are mean probabilities and their standard deviations over 1,000 iterations.

[b] Each analysis has a different class size of the *H. sapiens* group (see Methods section). For example, RF A has a reference class size of 3 HSA (HSA = 3) individuals selected at random.

Discussion

The six reconstructions of Kabua 1 vary in morphology, which is to be expected given the wide range of morphological variation among the reference crania (Bosman *et al.* 2019). As we show here, however, they are also substantially similar, providing a distribution of morphology that enables us to meaningfully discuss Kabua 1's taxonomic affinities. The closest neighbour (using Procrustes distances) of each reconstruction is another reconstruction, and none is particularly close to its reference model in shape space. This suggests there was sufficient anatomical information present to correctly place fragments separated due to taphonomic processes and that we are capturing a meaningful proportion of the shape of the original Kabua 1 fossil. Additionally, although we were constrained in the landmark data we could collect due to the preservation of Kabua 1 and the other fossils sampled, the landmarks we used were from regions that were well preserved in Kabua 1, making their placement more secure. Had we been able to collect a denser landmark set, covering more of the cranium, we may have been able to diagnose the affinities of Kabua 1 with greater precision. Nevertheless, globular neurocranial shape is considered a key diagnostic trait of derived *H. sapiens* (e.g., Athreya 2009; Harvati & Weaver 2006; Meneganzin *et al.* 2022; Mirazón Lahr 1996; 2016; Stringer 2016), and so analysis of this aspect of cranial variation is a valid means of assessing its affinity. By using a range of reference crania and discussing the distribution of potential shapes they suggest for Kabua 1, we avoid putting too much weight on any one particular reconstruction and its inherent biases. Indeed, such distribution of potential shapes is analogous to priors in a Bayesian framework (Gunz *et al.* 2009).

Our quantitative analyses support our previous, qualitative assessment of Kabua 1 (Bosman *et al.* 2019), showing that its morphological affinity lies largely with derived *H. sapiens*. At the same time, these new analyses applying diverse analytical methods also make it clear that the fossil's morphology diverges from this group in some respects. The position of the Kabua 1 reconstructions in the PCA (Figure 3) and the comparison of neurocranial shape indices support the hypothesis that its shape allies with *H. sapiens*. The PCA is informative because the grouping is merely overlain for visualization purposes and so our choice of group for the comparative sample does not influence the reconstructions' positions. It should be noted, however, that the PCA necessarily reduces the multidimensionality of shape to few variables and the results shown in Figure 3 and discussed in the text represent only ∼43% of total shape. On the other hand, there is considerable overlap in the comparison of neurocranial indices between *H. sapiens* and Middle Pleistocene African specimens (Figure 4), reducing the diagnostic power of this analysis. Such overlap reflects the great variation of neurocranial shape within our species, and potentially the equivocal position of some fossils such as Ngaloba and Saldanha, which have neurocranial morphology that places them between more basal and more derived parts of our lineage and has led to debate over their status as derived *H. sapiens*. Here we used broad, inclusive comparative groups as far as possible to avoid biases introduced by making taxonomic diagnoses (Brewster, Meiklejohn, Von Cramon-Taubadel & Pinhasi 2014; Harvati *et al.* 2011, 2019; Hublin *et al.* 2017). One could argue that dividing the *H. sapiens* group into Late Pleistocene specimens and recent Holocene sub-groups (see Table 2) would add valuable definition regarding the position of Kabua 1 within *H. sapiens*. However, the inclusion of additional groups with low sample sizes would reduce classification reliability due to multiple violations of minimal group size. Furthermore, given the

subsummation of the Late Pleistocene *H. sapiens* within the range of Holocene *H. sapiens* variation (SI Figure 5 in the Supporting Information), it seems likely there would be little to gain in terms of a more refined affinity for Kabua 1.

The Procrustes distance analyses (Figure 3, Table 5) broadly support the results of the PCA and neurocranial indices, as the reconstructions are closest neighbours to Late Pleistocene *H. sapiens* (Dolní Věstonice DV03) and recent, Holocene *H. sapiens* (South African 07, Turkana 01, and Zulu 13). The reconstruction based on Ngaloba is the exception, with Saldanha its closest neighbour in Procrustes distance. The reconstruction of Kabua 1 using Ngaloba as a reference cranium was difficult, since Ngaloba itself requires reconstruction from its constituent fragments, which do not articulate directly (Day *et al.* 1980), and there is some distortion of the frontal bone. In our virtual reconstruction of Ngaloba, we approximated the original reconstruction by Day *et al.* (1980) but note that the degree of facial prognathism will change depending on the positioning of the fragments (Bosman *et al.* 2019). The uncertainties inherent in this particular reconstruction of Kabua 1 could explain its greater proximity to Middle Pleistocene African specimens.

Our three classification techniques show somewhat different results to the PCA, neurocranial indices, and Procrustes distances. These methods are valuable partly for their inclusion of all (or all statistically significant – see Methods section) PCs, providing a more accurate reflection of total shape than the PCA. The linear discriminant analysis (LDA) was included to enable comparison with previous work. It classifies the majority of the Kabua 1 reconstructions as Middle Pleistocene Africans, with the exception of that based on Skhūl 5, which is classified as *H. sapiens*. LDA relies on the distance between a reconstruction (treated as a group with a single specimen) and the other group means, cross-validated with a leave-one-out procedure and can account for unequal sample sizes. It is, however, sensitive to deviations from normality and the presence of outliers (Hefner, Spradley & Anderson 2014), and assumption tests show that our PC data are non-normal and that our sample has several outliers, including two of the four Middle Pleistocene African specimens (SI Figure 4 in the Supporting Information). It should also be noted that LDA and related techniques are designed to maximize variance between groups, even attaining a separation between 'groups' in randomly generated data with no biological separation (Mitteroecker & Bookstein 2011). The grouping of all Middle Pleistocene Africans into a single class, with all their inherent variability and potentially different degrees of relatedness to *H. sapiens*, may inflate the problem. The results obtained using this method should be treated with caution, and yet, they are broadly supported by the other classification analyses.

k-nearest neighbour (*k*-NN) analyses are robust to deviations from normality and the inclusion of outliers, and they rely on Procrustes distances, which are computed from the Procrustes superimposed coordinates, resulting in a more complete picture than the LDA, which is based on only twelve significant principal components (see Methods section). Unequal sample sizes are a perennial problem in studies of fossil taxa, but here we attempted to account for the imbalance in class size by randomly subsampling the large *H. sapiens* sample (see section 2 in the Supporting Information). While most of the reconstructions classify primarily as *H. sapiens*, they also have high posterior probabilities of belonging to the Middle Pleistocene African group. The posterior probabilities for the other groups are zero because the maximal count of *k*-nearest neighbours is only three, preventing Neanderthal or Middle Pleistocene European specimens participating in the classification. The Kabua 1 reconstruction

based on Ngaloba classifies consistently as Middle Pleistocene African, confirming its low Procrustes distance to Saldanha. The Kabua 1 reconstruction using Kabwe 1 as a reference is classified as Middle Pleistocene African or *H. sapiens*, depending on the sample size of the *H. sapiens* group included. The *k*-NN shows a reasonably high Cohen's kappa score, reflecting tolerably low overlap between groups and wide intra-group variation.

Random forest (RF) models are also resistant to deviation from normality and outliers, and the random bagging of variables reduces the problem of multicollinearity without the need to apply ordination techniques, such as using the PC scores instead of the Procrustes coordinates. Even when we apply the RF models on the twelve significant PC scores, with exactly the same parameters as before, the results are similar to those presented here, albeit with lower Cohen's kappa scores (SI Table 3 in the Supporting Information). The RF models demonstrate correct classification percentages for the comparative sample and Cohen's kappa scores similar to, but slightly lower than, the *k*-NN models. The Ngaloba- and Kabwe 1-based Kabua reconstructions are classified primarily as Middle Pleistocene African, the reconstruction based on Skhūl 5 classifies primarily as *H. sapiens*, and the other three reconstructions variably classify as either group across the different models (Table 8). As the number of randomly subsampled *H. sapiens* is increased, the reconstructions are more likely to be classified as members of this group, demonstrating the effect of the class imbalance problem.

Machine learning methods, such as *k*-NN and RF, are not often applied to geometric morphometric studies in palaeoanthropology (Hefner *et al.* 2014); yet, they appear effective in classifying unknown individuals on the basis of neurocranial shape, even in a dataset with high intra-group variation. As these methods can provide robust alternatives to the aforementioned problems associated with LDA (Hefner *et al.* 2014; Navega *et al.* 2015), their potential should be further explored. One downside of these methods, however, is that they are influenced by their training set, which is unavoidably small for fossil groups due to the sparse fossil record and availability of 3D data. Violations of minimum group size and the class imbalance problem can negatively affect any machine learning model, reducing overall classification confidence. While techniques exist to artificially oversample small groups to better train machine learning models (Chawla, Bowyer, Hall & Kegelmeyer 2002; Japkowicz 2000), they do not reflect the morphological variation among actual fossil specimens, and their reliability for geometric morphometric data remains untested. Given these potential issues, the classifications provided by the LDA, *k*-NN, and RF models presented here should be treated with caution and compared with results from the ordination analyses presented above, which have less power to reveal diagnostic morphology but are not dependent on group sample size or taxonomic groupings.

The results we present here support the contention of previous authors that Kabua 1 lies within the broad taxon *H. sapiens* (Bosman *et al.* 2019; Rightmire 1975; Schepartz 1987). Through the quantitative analyses presented here, we can now add that, although Kabua 1 shows largely derived *H. sapiens* characteristics, it retains morphology that leads to its classification with Middle Pleistocene African hominins in some analyses. In this regard, it is somewhat similar to fossils from Hofmeyr (South Africa) and Nazlet Khater (Egypt), both dated from ~38 ka to 36 ka. Although these two crania present a suite of features that align them with derived *H. sapiens*, they also exhibit more basal features (Crevecoeur, Rougier, Grine & Froment 2009; Crevecoeur & Trinkaus 2004; Grine 2023; Grine *et al.* 2007). For example, Nazlet Khater 2 shows

an extremely large, broad face and an exceptionally robust, broad mandibular ramus reminiscent of European and African Middle Pleistocene hominins (Crevecoeur *et al.* 2009; Crevecoeur & Trinkaus 2004). Likewise, Hofmeyr has a continuous supraorbital torus, which is very rare in derived *H. sapiens* (but is also present in a few other Late Pleistocene *H. sapiens*, such as Skhūl V) (Crevecoeur *et al.* 2009; Grine 2023).

Such high levels of phenotypic variation within Africa are geographically widespread and retained throughout the Late Pleistocene, as demonstrated by fossils such as Ishango (~20-25 ka), and Lukenya Hill (~22 ka) and Iwo Eleru (~14 ka) (Crevecoeur *et al.* 2009; 2016; Harvati *et al.* 2011; Stringer 2016; Tryon *et al.* 2015). With the new conservative U-series minimum date of ~65 ka and our geometric morphometric analyses, we might now add Kabua 1 to this group of phenotypically highly variable fossil *H. sapiens* from Late Pleistocene Africa. Further to the relatively deeper history of our species in Africa and the consequent larger population size and genetic diversity of living Africans, prehistoric intra-African population expansions and contractions, interbreeding with other hominin taxa, or the retention of deep population structure may have contributed to the phenotypic diversity observed (Garrigan & Hammer 2006; Harvati *et al.* 2011, 2024; Mirazón Lahr 2016; Scerri *et al.* 2018; 2019). Importantly, given that the global variation to which we compare African phenotypic diversity is depauperate due to multiple founders' effects, it is likely that with these diverse African fossils we are beginning to sample previously uncharacterized variation within *H. sapiens*. Further studies of the levels and patterns of intraspecific variation in non-human primates (e.g., Buck *et al.* 2019; Harvati, Frost & McNulty 2004; Stock & Buck 2010; Zichello, Baab, McNulty, Raxworthy & Steiper 2018) and those bringing the tools of virtual anthropology to 'forgotten', fragmentary fossils such as Kabua 1 may help to determine if this level of variation is atypical of a widespread species. Further investigation of the Kabua fossil, including analysis of the mandible and teeth, as well as of its brain and inner ear endocasts, will also serve to clarify its affinities to Middle to Late Pleistocene fossils.

Acknowledgements

We thank the institutions holding the sample used here and their staff for access/permission to use their data and for support during data collection/transfer: Support for this research was provided by the German Research Foundation (Deutsche Forschungsgemeinschaft, DFG FOR 2237: Project 'Words, Bones, Genes, Tools: Tracking Linguistic, Cultural, and Biological Trajectories of the Human Past' and DFG INST 37/706-1 FUGG: Paleoanthropology High Resolution CT Laboratory). Laura Buck was additionally supported by the Human Origins Research Fund of the Natural History Museum, London. Katarina Harvati is supported by the ERC Consolidator Grant CROSSROADS #724703 and Advanced Grant FIRSTSTEPS #101019659, the DFG Leibniz award 2021, and the Carl Friedrich von Siemens Foundation. Chris Stringer's research is supported by the Calleva Foundation and the Human Origins Research Fund and this paper is a contribution to the NHM's Evolution of Life research theme. Hugo Reyes-Centeno is supported by the US National Science Foundation (Mid-scale RI-1 2131940, EduceLab: Infrastructure for Next-Generation Heritage Science) and the Swedish Research Council (VR Center of Excellence, the Center for the Human Past, grant number 2022-06620_VR). Marta Mirazón Lahr's research is supported by the ERC Advanced Grants IN-AFRICA #295907 and NGIPALAJEM #101020478.

NOTE

[1] Species diagnosis of *H. sapiens* is not straightforward. Here we will not consider those who argue for a very wide diagnosis that includes groups like the Neanderthals. To simplify, most researchers disagree over whether to include everything on our own taxonomic branch after our divergence from our last common ancestor with Neanderthals, or solely the tip of that branch where individuals have the full complement of diagnostic traits seen in recent/living people (Stringer 2016; Stringer & Buck 2014). Here we use the terms 'basal' to describe the former group and 'derived' to describe the latter (Bermúdez de Castro & Martinón-Torres 2022; Stringer & Crete 2022). These terms are broadly comparable to the way many authors use the terms 'archaic' and '(anatomically) modern' in discussions of *H. sapiens* but are less burdened by potentially pejorative connotations, an implied progressive view of evolution, and, in the case of 'archaic', by historic use of the term for a much broader group of fossils that would now generally be placed in different taxa, e.g., Neanderthals (Stringer 2012; Stringer & Buck 2014). Of course, if the very deep split times of >1 Ma inferred by Feng *et al.* (2025) are accurate, then even the term basal *sapiens* may not be adequate to encompass the degree of difference from derived *H. sapiens* expected in the earliest members of the lineage.

REFERENCES

Adams, D.C. & E. Otárola-Castillo 2013. geomorph: an r package for the collection and analysis of geometric morphometric shape data. *Methods in Ecology and Evolution* **4**, 393-9.

Athreya, S. 2009. A comparative study of frontal bone morphology among Pleistocene hominin fossil groups. *Journal of Human Evolution* **57**, 786-804.

——— & A. Hopkins 2021. Conceptual issues in hominin taxonomy: *Homo heidelbergensis* and an ethnobiological reframing of species. *American Journal of Physical Anthropology* **175**, 4-26.

Auer, P. & D. Gervini 2008. Choosing principal components: a new graphical method based on Bayesian model selection. *Communications in Statistics – Simulation and Computation* **37**, 962-77.

Bergström, A., C. Stringer, M. Hajdinjak, E.M.L. Scerri & P. Skoglund 2021. Origins of modern human ancestry. *Nature* **590**, 229-37.

Bermúdez de Castro, J.M. & M. Martinón-Torres 2022. The origin of the *Homo sapiens* lineage: when and where? *Quaternary International* **634**, 1-13.

Bookstein, F.L. 1989. Principal warps: thin-plate splines and the decomposition of deformations. *IEEE Transactions on Pattern Analysis and Machine Intelligence* **11**, 567-85.

Bosman, A.M., L.T. Buck, H. Reyes-Centeno, *et al.* 2019. The Kabua 1 cranium: virtual anatomical reconstructions. In *Modern human origins and dispersals* (eds) Y. Sahle, H. Reyes-Centeno & C. Bentz, 137-70. Tübingen: Kerns Verlag.

Bräuer, G. 1976. Morphological and multivariate analysis of human skeletons from Iron Age graves northeast of Lake Eyasi (Tanzania). *Homo* **27**, 185-96.

Breiman, L. 2001. Random forests. *Machine Learning* **45**, 5-32.

Brewster, C., C. Meiklejohn, N. Von Cramon-Taubadel & R. Pinhasi 2014. Craniometric analysis of European Upper Palaeolithic and Mesolithic samples supports discontinuity at the Last Glacial Maximum. *Nature Communications* **5**, 4094.

Buck, L.T., I. De Groote, Y. Hamada, *et al.* 2019. Evidence of different climatic adaptation strategies in humans and non-human primates. *Scientific Reports* **9**, 11025.

——— & C.B. Stringer 2014. Quick guide to *Homo heidelbergensis*. *Current Biology* **24**, R14-R15.

Chan, E.K.F., A. Timmermann, B.F. Baldi, *et al.* 2019. Human origins in a southern African palaeo-wetland and first migrations. *Nature* **575**, 185-9.

Chawla, N.V., K.W. Bowyer, L.O. Hall & W.P. Kegelmeyer 2002. SMOTE: synthetic minority over-sampling technique. *Journal of Artificial Intelligence Research* **16**, 321-57.

Claude, J. 2008. *Morphometrics with R*. New York: Springer.

Cousins, T., A. Scally & R. Durbin 2025. A structured coalescent model reveals deep ancestral structure shared by all modern humans. *Nature Genetics* **57**, 856-64.

Crevecoeur, I., I.A. Brooks, I. Ribot, E. Cornelissen & P. Semal 2016. Late Stone Age human remains from Ishango (Democratic Republic of Congo): new insights on Late Pleistocene modern human diversity in Africa. *Journal of Human Evolution* **96**, 35-75.

———, H. Rougier, F. Grine & A. Froment 2009. Modern human cranial diversity in the late Pleistocene of Africa and Eurasia: evidence from Nazlet Khater, Peştera cu Oase, and Hofmeyr. *American Journal of Physical Anthropology* **140**, 347-58.

——— & E. Trinkaus 2004. From the Nile to the Danube: a comparison of the Nazlet Khater 2 and Oase 1 early modern human mandibles. *Anthropologie* **42**, 203-14.
Day, M.H., M.D. Leakey & C. Magori 1980. A new hominid fossil skull (L.H. 18) from the Ngaloba Beds, Laetoli, northern Tanzania. *Nature* **284**, 55-6.
Delson, E. & C. Stringer 2022. The naming of *Homo bodoensis* by Roksandic and colleagues does not resolve issues surrounding Middle Pleistocene human evolution. *Evolutionary Anthropology* **31**, 233-6.
Feng, X., Q. Yin, F. Gao, *et al.* 2025. The phylogenetic position of the Yunxian cranium elucidates the origin of *Homo longi* and the Denisovans. *Science* **389: 6767**, 1320-4.
Fligner, M.A. & T.J. Killeen 1976. Distribution-free two-sample tests for scale. *Journal of the American Statistical Association* **71**, 210-13.
Garrigan, D. & M.F. Hammer 2006. Reconstructing human origins in the genomic era. *Nature Reviews Genetics* **7**, 669-80.
Grine, F.E. 2023. *Hofmeyr: a Late Pleistocene human skull from South Africa*. Cham: Springer International.
———, R. M. Bailey, K. Harvati, R.P. Nathan, A.G. Morris, H.M. Henderson, I. Ribot & A.W. Pike 2007. Late Pleistocene human skull from Hofmeyr, South Africa, and modern human origins. *Science*, **315**, 226-9.
Grün, R., J.S. Brink, N.A. Spooner, *et al.* 1996. Direct dating of Florisbad hominid. *Nature* **382**, 500-1.
———, S. Eggins, L. Kinsley, H. Moseley & M. Sambridge 2014. Laser ablation U-series analysis of fossil bones and teeth. *Palaeogeography, Palaeoclimatology, Palaeoecology* **416**, 150-67.
———, A. Pike, F. McDermott, *et al.* 2020. Dating the skull from Broken Hill, Zambia, and its position in human evolution. *Nature* **580**, 372-5.
———, C. Stringer, F. McDermott, *et al.* 2005. U-series and ESR analyses of bones and teeth relating to the human burials from Skhul. *Journal of Human Evolution* **49**, 316-34.
Gunz, P., P. Mitteroecker, S. Neubauer, G.W. Weber & F.L. Bookstein 2009. Principles for the virtual reconstruction of hominin crania. *Journal of Human Evolution* **57**, 48-62.
Harding, R.M. & G. McVean 2004. A structured ancestral population for the evolution of modern humans. *Current Opinion in Genetics and Development* **14**, 667-74.
Harvati, K. 2007. 100 years of *Homo heidelbergensis* – life and times of a controversial taxon. *Mitteilungen der Gesellschaft fur Urgeschichte* **16**, 85-94.
——— 2009. Into Eurasia: a geometric morphometric re-assessment of the Upper Cave (Zhoukoudian) specimens. *Journal of Human Evolution*, **57**, 751-62.
——— & R.R. Ackermann 2022. Merging morphological and genetic evidence to assess hybridization in Western Eurasian late Pleistocene hominins. *Nature Ecology & Evolution* **6**, 1573-85.
———, S.R. Frost, K.P. McNulty 2004. Neanderthal taxonomy reconsidered: implications of 3D primate models of intra- and interspecific differences. *Proceedings of the National Academy of Sciences USA* **101**, 1147-52.
———, P. Gunz & D. Grigorescu 2007. Cioclovina (Romania): affinities of an early modern European. *Journal of Human Evolution* **53**, 732-46.
——— & H. Reyes-Centeno 2022. Evolution of *Homo* in the Middle and Late Pleistocene. *Journal of Human Evolution* **173**, 103279.
———, C. Röding, A.M. Bosman, e*t al.* 2019. Apidima Cave fossils provide earliest evidence of *Homo sapiens* in Eurasia. *Nature* **571**, 500-4.
———, C. Stringer & C.A. Folorunso 2024. Comparative 3D shape analysis of the Iwo Eleru mandible, Nigeria. *PaleoAnthropology* **1**, 99-111.
———, C. Stringer, R. Grün, *et al.* 2011. The later stone age calvaria from Iwo Eleru, Nigeria: morphology and chronology. *PLoS ONE* **6**, e24024.
——— & T.D. Weaver 2006. Human cranial anatomy and the differential preservation of population history and climate signatures. *Anatomical Record* **288**, 1225-33.
Hautavoine, H., J. Arnaud, A. Balzeau & A. Mounier 2024. Quantifying hominin morphological diversity at the end of the Middle Pleistocene: implications for the origin of *Homo sapiens*. *American Journal of Biological Anthropology* **184**, 24915.
Hefner, J.T., M.K. Spradley & B. Anderson 2014. Ancestry assessment using random forest modeling. *Journal of Forensic Sciences* **59**, 583-9.
Henn, B.M., T.E. Steele & T.D. Weaver 2018. Clarifying distinct models of modern human origins in Africa. *Current Opinion in Genetics & Development* **53**, 148-56.
Howell, F.C. 1999. Paleo-demes, species clades, and extinctions in the Pleistocene hominin record. *Journal of Anthropological Research* **55**, 191-243.

Hubbe, M., T. Hanihara & K. Harvati 2009. Climate signatures in the morphological differentiation of worldwide modern human populations. *Anatomical Record* **292**, 1720-33.

Hublin, J.-J. 2007. What can Neanderthals tell us about modern human origins? In *Rethinking the human revolution* (eds) P. Mellars, K. Boyle, O. Bar-Yosef & C. Stringer, 235-48. Cambridge: McDonald Institute Monographs.

———, A. Ben-Ncer, S.E. Bailey, *et al.* 2017. New fossils from Jebel Irhoud, Morocco and the pan-African origin of *Homo sapiens*. *Nature* **546**, 289-92.

Immersion Corporation 1998. Microscribe 3D.

Japkowicz, N. 2000. The class imbalance problem: significance and strategies. In *Proceedings of the 2000 international conference on artificial intelligence (IC-AI'2000): special track on inductive learning, Las Vegas*. Las Vegas, Nevada.

Kuhn, M. 2007. caret: Classification and Regression Training. *https://cran.r-project.org/web/packages/caret/caret.pdf*.

——— 2008. Building predictive models in R using the caret package. *Journal of Statistical Software* **28: 5**, 1–26.

Mardia, K.V. & P.E. Jupp 2000. *Directional statistics*. Chichester: Wiley.

Mehlman, M.J. 1979. Mumba-Höhle revisited: the relevance of a forgotten excavation to some current issues in east African prehistory. *World Archaeology* **11**, 80-94.

Meneganzin, A., T. Pievani & G. Manzi 2022. Pan-Africanism vs. single-origin of *Homo sapiens*: putting the debate in the light of evolutionary biology. *Evolutionary Anthropology* **31**, 199-212.

Mirazón Lahr, M. 1996. *The evolution of modern human diversity: a study of cranial variation*. Cambridge: University Press.

——— 2016. The shaping of human diversity: filters, boundaries and transitions. *Philosophical Transactions of the Royal Society B: Biological Sciences* **371**, 20150241.

Mitteroecker, P. & F. Bookstein 2011. Linear discrimination, ordination, and the visualization of selection gradients in modern morphometrics. *Evolutionary Biology* **38**, 100-14.

Navega, D., C. Coelho, R. Vicente, *et al.* 2015. AncesTrees: ancestry estimation with randomized decision trees. *International Journal of Legal Medicine* **129**, 1145-53.

Perez, S.I., V. Bernal & P.N. Gonzalez 2006. Differences between sliding semi-landmark methods in geometric morphometrics, with an application to human craniofacial and dental variation. *Journal of Anatomy* **208**, 769-84.

Phenice, T.W. & N.J. Sauer 1977. *Hominid fossils: an illustrated key*. Dubuque, Iowa: W.C. Brown.

R Core Team 2019. *R: a language and environment for statistical computing*. Vienna: R Foundation for Statistical Computing.

Ragsdale, A.P., T.D. Weaver, E.G. Atkinson, et al. 2023. A weakly structured stem for human origins in Africa. *Nature* **617**, 755-63.

Reyes-Centeno, H., L. Buck, C. Stringer & K. Harvati 2014. The inner ear of the Eyasi I (Tanzania) and Kabua I (Kenya) hominin fossils. Paper presented at The African human fossil record. Toulouse.

Richter, D., R. Grün, R. Joannes-Boyau, et al. 2017. The age of the hominin fossils from Jebel Irhoud, Morocco, and the origins of the Middle Stone Age. *Nature* **546**, 293-6.

Rightmire, G.P. 1975. New studies of post-Pleistocene human skeletal remains from the Rift Valley, Kenya. *American Journal of Physical Anthropology* **42**, 351-69.

Ripley, B.D. 1996. *Pattern recognition and neural networks*. Cambridge: University Press.

Roksandic, M., P. Radović, X.J. Wu & C.J. Bae 2022. Resolving the 'muddle in the middle': the case for *Homo bodoensis* sp. nov. *Evolutionary Anthropology* **31**, 20-9.

Scerri, E.M.L., L. Chikhi & M.G. Thomas 2019. Beyond multiregional and simple out-of-Africa models of human evolution. *Nature Ecology and Evolution* **3**, 1370-2.

———, M.G. Thomas, A. Manica, et al. 2018. Did our species evolve in subdivided populations across Africa, and why does it matter? *Trends in Ecology & Evolution* **33**, 582-94.

Schepartz, L.A. 1987. *From hunters to herders: subsistence pattern and morphological change in eastern Africa*. PhD thesis, University of Michigan, Ann Arbor.

Schlebusch, C.M., L. Loog, H.S. Groucutt, *et al.* 2021. Human origins in Southern African palaeo-wetlands? Strong claims from weak evidence. *Journal of Archaeological Science* **130**, 105374.

Spoor, F., C. Stringer & F. Zonneveld 1998. Rare temporal bone pathology of the Singa calvaria from Sudan. *American Journal of Physical Anthropology* **107**, 41-50.

Stock, J.T. & L.T. Buck 2010. Canalization and plasticity in humans and primates: implications for interpreting the fossil record. In *150 años después de Darwin: Evolución, future o crisis? Lecciones sobre*

evolución humana (eds) A.P. Alejandre & A.M. Cachorro, 91-101. Madrid: Instituto Tomás Pascual Sanz.
Stringer, C. 2002. Modern human origins: progress and prospects. *Philosophical Transactions of the Royal Society B: Biological Sciences* **357**, 563-79.
——— 2012*a*. What makes a modern human? *Nature* **485**, 33-5.
——— 2012*b*. The status of *Homo heidelbergensis* (Schoetensack 1908). *Evolutionary Anthropology* **21**, 101-7.
——— 2016. The origin and evolution of *Homo sapiens*. *Philosophical Transactions of the Royal Society B: Biological Sciences* **371**, 20150237.
——— 2022. The development of ideas about a recent African origin for *Homo sapiens*. *Journal of Anthropological Sciences* **100**, 5-18.
——— & L.T. Buck 2014. Diagnosing *Homo sapiens* in the fossil record. *Annals of Human Biology* **41**, 312-22.
——— & L. Crete 2022. Mapping interactions of *Homo neanderthalensis* and *Homo sapiens* from the fossil and genetic records. *PaleoAnthropology* **2022**, 401-12.
———, J.-J. Hublin & B. Vandermeersch 1984. The origin of anatomically modern humans in Western Europe. In *The origins of modern humans: a world survey of the fossil evidence* (eds) F.H. Smith & F. Spencer, 51-135. New York: Liss.
Thermo Fisher Scientific 2019. Avizo Lite 9.0.
Tryon, C.A., I. Crevecoeur, J.T. Faith, *et al.* 2015. Late Pleistocene age and archaeological context for the hominin calvaria from GvJm-22 (Lukenya Hill, Kenya). *Proceedings of the National Academy of Sciences USA* **112**, 2682-7.
Venables, W.N. & B.D. Ripley 2002. *Modern applied statistics with S*. (4th edition.) New York: Springer.
Vidal, C.M., C.S. Lane, A. Asrat, et al. 2022. Age of the oldest known *Homo sapiens* from eastern Africa. *Nature* **601**, 579-83.
Wang, M., S.M. Kornblau & K.R. Coombes 2018. Decomposing the apoptosis pathway into biologically interpretable principal components. *Cancer Informatics* **17**, 1176935118771082.
Weber, G.W. & F.L. Bookstein 2011. *Virtual anthropology: a guide to a new interdisciplinary field*. New York: Springer.
Whitworth, T. 1960. Fossilized human remains from Northern Kenya. *Nature* **185**, 947-8.
——— 1966. A fossil hominid from Rudolf. *South African Archaeological Bulletin* **21**, 138-50.
Wickham, H. 2016. Data analysis. In *ggplot2: elegant graphics for data analysis*, 189-201. Cham: Springer International.
Wright, M.N. & A. Ziegler 2017. ranger: a fast implementation of random forests for high dimensional data in C++ and R. *Journal of Statistical Software* **77**, 1-17.
Zichello, J.M., K. Baab, K. McNulty, C. Raxworthy & M. Steiper 2018. Hominoid intraspecific cranial variation mirrors neutral genetic diversity. *Proceedings of the National Academy of Sciences USA* **45**, 11501-6.

Affinités morphologiques du crâne fossile de Kabua (Kenya)

Résumé

Notre compréhension actuelle des origines d'*Homo sapiens* est limitée, en partie, par les lacunes des traces fossiles du Pléistocène tardif et de l'Holocène précoce en Afrique. Les auteurs réexaminent ici le crâne Kabua 1, fossile énigmatique et peu étudié qui fut découvert au Kenya dans les années 1950. Afin d'étudier ses affinités morphologiques, l'équipe compare des reconstitutions en images de synthèse qu'elle a réalisées antérieurement à un large assortiment de fossiles datant du Pléistocène moyen à l'Holocène précoce, ainsi qu'à des crânes d'*H. sapiens* africains récents. Les auteurs proposent également une nouvelle datation par les séries de l'uranium, conservatrice, de 64,4 ± 5,4 ka au minimum. Les résultats mettent en lumière les larges similitudes entre Kabua 1 et les dérivés d'*H. sapiens*, récents aussi bien que fossiles. Toutefois, la morphologie de ce fossile montre certaines affinités plus basales et contribue ainsi à notre compréhension de la vaste diversité phénotypique d'*H. sapiens* au Pléistocène tardif en Afrique.

Abel Marinus Bosman completed his PhD as part of the DFG Centre for Advanced Studies 'Words, Bones, Genes, Tools' at Eberhard Karls Universität Tübingen in 2019. He is now a Project Manager and Coordinating Policy Officer at the Ministry of Infrastructure and Water Management in the Netherlands, with a focus on smart mobility and public sector digital innovation.

Laura Tabitha Buck is a Senior Lecturer in Evolutionary Anthropology and co-Lead of the Research Centre for Evolutionary Anthropology and Palaeoecology at Liverpool John Moores University. This work was begun when she was a Fellow of the DFG Centre for Advanced Studies 'Words, Bones, Genes, Tools' at Eberhard Karls Universität Tübingen and a Scientific Associate of the Human Origins Group at the Natural History Museum, London. Her main research currently concerns understanding the morphological consequences of hybridization between humans and Neanderthals.

Hugo Reyes-Centeno is Assistant Professor of Anthropology at the University of Kentucky and Co-Principal Investigator of EduceLab, a US National Science Foundation Mid-Scale Infrastructure for Next-Generation Heritage Science. Hugo studies the emergence of modern human anatomy and the association between anatomical, genomic, and linguistic diversity over the last million years of human evolution.

Marta Mirazón Lahr is Professor of Human Evolutionary Biology and Prehistory in the Department of Archaeology at the University of Cambridge. Her research concerns human evolution and prehistory, especially the evolution of modern humans in Africa; the evolution of human diversity; African biogeography; multi-disciplinary and integrated approaches to the human past.

Chris Stringer is a Scientific Associate in the Centre for Human Evolutionary Research (CHER) at the Natural History Museum, London. His early research was on the relationship of Neanderthals and early *Homo sapiens* in Europe, but he now collaborates with palaeontologists, archaeologists, Earth scientists and geneticists in attempting to reconstruct the evolution of humans globally.

Rainer Grün is Emeritus Professor at The Australian National University, and is also affiliated with the School of Geography, Nanjing Normal University, China. During the period when this work was conducted, he held a Fellowship at the DFG Centre for Advanced Studies 'Words, Bones, Genes, Tools' at Eberhard Karls Universität Tübingen. His research interests centre on the development of dating methods, particularly ESR and U-series dating, and the application of these methods to key questions in Quaternary research.

Qingfeng Shao is a professor in School of Geography, Nanjing Normal University, Nanjing, China. He is mainly interested in the development of U-series dating method and the applications in Archaeology and Palaeoanthropology.

Katerina Harvati is Professor of Palaeoanthropology and Director of the Senckenberg Center for Human Evolution and Environment at Eberhard Karls Universität Tübingen. Her research focuses on Neanderthal evolution, modern human origins, and the application of 3-D geometric morphometrics and virtual anthropology to paleoanthropology.